第 30 卷第 6 期
2014 年 6 月

无 机 化 学 学 报
CHINESE JOURNAL OF INORGANIC CHEMISTRY

Vol.30 No.6
1352-1360

低温溶剂热法制备 5 V 级性能优异的 $LiCr_{0.2}Ni_{0.4}Mn_{1.4}O_4$ 正极材料

陈明哲[1] 钟艳君[1] 张 辉[2] 何宾宾[2] 钟本和[1] 郭孝东*,[1]

([1]四川大学化学工程学院,成都 610065)

([2]云南磷化集团有限公司,昆明 650600)

摘要：通过低温溶剂热的方法成功制备出了 $LiCr_{0.2}Ni_{0.4}Mn_{1.4}O_4$ 尖晶石正极材料。通过此法,溶液的饱和蒸汽压急剧降低且在室温(25℃)下即可沸腾。所有的金属离子可在随后的热聚合过程中均匀分散且煅烧后所得材料无杂质相生成。采用了热重分析,X 射线衍射,扫描电镜、循环伏安,交流阻抗等测试手段对材料进行了表征。结果表明:此法所得材料含有 Mn^{3+},为 $Fd\bar{3}m$ 晶型,且其形貌规则、粒度分布均一。1C 和 10C 下放电容量为 140.5 和 121.0 mAh·g^{-1},10C 下 100 次循环容量保持率高达 96.9%。其优异的电化学性能可归因于均相的前驱体制备过程,高结晶度且无杂相生成,以及较高的锂离子扩散系数诸因素的共同作用。

关键词：5 V 级尖晶石 $LiCr_{0.2}Ni_{0.4}Mn_{1.4}O_4$；电化学性能；低温溶剂热法；锂离子电池

中图分类号：O646；TQ139.2 **文献标识码**：A **文章编号**：1001-4861(2014)06-1352-09

DOI:10.11862/CJIC.2014.197

Superior Electrochemical Properties of 5 V $LiCr_{0.2}Ni_{0.4}Mn_{1.4}O_4$ Cathode Material Prepared by Low-Temperature Solvothermal Method

CHEN Ming-Zhe[1] ZHONG Yan-Jun[1] ZHANG Hui[2] HE Bin-Bin[2]

ZHONG Ben-He[1] GUO Xiao-Dong*,[1]

([1]*College of Chemical Engineering, Sichuan University, Chengdu* 610065, *China*)

([2]*Yunnan Phosphate Chemical Group CO., LTD, Kunmin* 650600, *China*)

Abstract: The Cr-doped spinel $LiCr_{0.2}Ni_{0.4}Mn_{1.4}O_4$ cathode material has been synthesized by a low-temperature solvothermal method. Via this way, the saturated vapor pressure of the solution could be sharply reduced and the ebullition of whole solution can occur at room temperature (25 ℃). All metal ions are able to be dispersed at a homogeneous state during the subsequent thermal polymerization process without formation of any impurity. Various measurements were used for investigating the morphology, structure, physical property and electrochemical performances, including thermal gravimetric analysis (TG), X-ray diffraction (XRD), scanning electron microscopy (SEM), cyclic voltammetry (CV) and electrochemical impedance spectroscopy (EIS), etc. The results reveal that the sample synthesized by low-temperature solvothermal method has a space group of $Fd\bar{3}m$ within a small amount of Mn^{3+} and well-shaped morphology with uniform size distribution. Electrochemical test shows that the as-prepared sample exhibits an excellent discharge capacity of 140.5 and 121.0 mAh·g^{-1} at 1C and 10C, respectively. Moreover, a stable cyclic performance is demonstrated by desirable capacity retention of 96.9% after 100 cycles at 10C. In summary, homogeneous state during precursor preparation, high crystallinity and structure stability with no impurities, and superior diffusion coefficient of Li^+ together make great contribution to the enhanced electrochemical performances of the as-synthesized sample.

Key words: 5 V Spinel $LiCr_{0.2}Ni_{0.4}Mn_{1.4}O_4$; Electrochemical performance; Low-temperature solvothermal method; Lithium ion battery

收稿日期:2013-11-20。收修改稿日期:2014-02-05。

四川大学青年基金资助项目(No.2011SCU11081);教育部高校博士学科点科研基金(No.20120181120103);磷化工国家工程中心开放基金项目(No.2013LF1012)。

*通讯联系人。E-mail:xiaodong2009@scu.edu.cn

0 Introduction

Recently, lithium-ion batteries (LIBs) as the most widely used and promising energy source have shown great value for their characteristics of rechargeable and long lifespan, while being environmentally benign and having a high energy density[1]. In the field of cathode, the Ni-doped manganese spinel oxide-$LiNi_{0.5}Mn_{1.5}O_4$ has gained attentions of lots of researchers as it provides an access to get high voltage (around 4.7 V) and high theoretic specific capacity (146.7 mAh·g^{-1})[2] via unique three-dimensional Li^+ diffusion channels[3]. Nevertheless, impurity phases such as $Li_xNi_{1-x}O$, NiO could easily form in the structure during synthesis, which can lead to capacity loss[4]. Several approaches have been taken to overcome these drawbacks[5-6], including partial replacement of Ni and Mn by Cr[5,7]. The bonding energy of Cr-O (461 kJ·mol^{-1}) is stronger than that of Ni-O (382 kJ·mol^{-1}) and Mn-O (402 kJ·mol^{-1}), therefore the formation of impurities can be effectively suppressed by reducing oxygen loss during high-temperature calcination[7]. Besides, the addition of Cr^{3+} enable $LiCr_{2x}Ni_{0.5-x}Mn_{1.5-x}O_4$ to de-/inserted Li^+ at a higher potential ($E\approx4.75$~4.8 V vs Li/Li^+) than that of $LiNi_{0.5}Mn_{1.5}O_4$ (E=4.7 V vs Li/Li^+) which ascribe to Cr^{3+}/Cr^{4+} redox couple ($E\approx4.9$ V vs Li/Li^+)[6,8]. On the other hand, numerous researchers have been focusing on the optimum synthesis conditions[9], and a variety of synthetic routes for this material have been developed up to now, such as co-precipitation[10-11], sol-gel[12-14], solid state reaction[15-16], combustion[17-18], molten salt method[19], spray pyrolysis[20], etc. In order to get a simple and easy to be industrialized approach without consuming a lot of heat energy, we have synthesized $LiCr_{0.2}Ni_{0.4}Mn_{1.4}O_4$ cathode material via a method of low-temperature solvothermal process. By using this approach, (i) the solution′s saturated vapor pressure could be sharply reduced and the ebullition of whole solution can occur at room temperature (25 ℃); (ii) The hydrolysis level of metal ions can be minimized; (iii) the generated bubbles may have effect on the subsequent thermal polymerization process. The physicochemical and electrochemical performances of sintered materials were investigated in detail.

To the best of our knowledge, the aforementioned synthetic route has not ever been reported[21-24]. As a simple and readily accessible route without regulating pH value or adding organic chelating agents[25], it also has other advantages in industrialized production when compared with other routes, such as low-cost and high stability of different batches of products.

1 Experimental

1.1 Synthesis of $LiCr_{0.2}Ni_{0.4}Mn_{1.4}O_4$

The particles of $LiCr_{0.2}Ni_{0.4}Mn_{1.4}O_4$ cathode material was synthesized by the low-temperature solvothermal method. Stoichiometric amounts of all nitrate ($LiNO_3$, $Ni(NO_3)_2\cdot6H_2O$, $Cr(NO_3)_3\cdot9H_2O$) apart from acetate of manganese ($Mn(Ac)_2\cdot4H_2O$) were dissolved in deionized water. Sucrose as dispersing agent was also added in the solution (the mole ratio of sucrose and all metal ions is 1∶1). After stirring continuously for 1 h, the solution was transferred to a high-vacuum device so that the redundant solvent can be removed at room temperature (25 ℃). Then viscous solution was poured into a crucible and kept in a vacuum drying chamber at 120 ℃ for 12 h in order to complete the reaction of thermo polymerization (These prepared procedures were schematically illustrated in Fig.1.). After being ground up into powder, the precursor was sintered at 900 ℃ for 1 h in the air to obtain spinel $LiCr_{0.2}Ni_{0.4}Mn_{1.4}O_4$ product, which was named Sample A. For the sake of comparison, the material obtained via the same procedure but

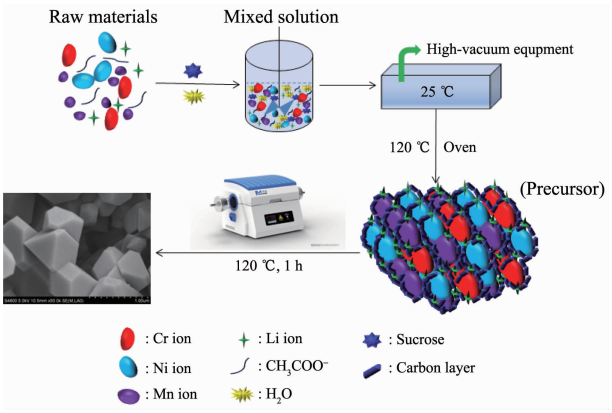

Fig.1 Flow chart of the low-temperture solvothermal method

synthesized by low-temperature solvothermal method (90 ℃) was named Sample B. All of the chemicals used were the grade of analytical reagent, and in order to make up the evaporative loss of lithium during calcination, the amount of $LiNO_3$ was in excess of 5%.

1.2 Physical characterization and electrochemical measurements

The cathode was produced by mixing the as-synthesized $LiCr_{0.2}Ni_{0.4}Mn_{1.4}O_4$ material, polyvinylidene fluoride (PVDF, blinder) and acetylene black, with mass fraction of 80wt%, 7wt%, 13wt%, respectively. The electrolyte used for electrochemical test consists of a solution of 1mol·L^{-1} $LiPF_6$ in ethylene carbonate (EC) with identical dimethyl carbonate (DMC) in volume, and Celgard 2300 was used as a separator between anode (lithium) and cathode. All the button cells were assembled in a glove box filled with argon.

Thermogravimetric analysis was operated on a thermogravimetric analyzer (NETZSCH, TG 2091) with a heating rate of 10 ℃·min^{-1} to determine the mass loss and thermal behaviors. The purity and crystal structure were detected by X-ray diffraction (XRD, DX-1000 Cu $K\alpha$, the 2θ ranges from 10° to 70° with a scanning speed of 0.026°·s^{-1}). The particle size distribution measurement results were showed by a laser particle size distribution tester (JL-6000) (wet method). The morphological examinations of two prepared samples were made by a scanning electron microscope (SEM, HITACHI S-4800). Electrochemical tests were carried out in the potential range of 3.6~5.0 V with a battery test device (Neware BTS-610) at room temperature (25 ℃). Electrochemical impedance spectrum (EIS) was measured by an eletrochemical workstation in a frequency range of 100 kHz ~10 mHz, and the amplitude of AC voltage was 5 mV. Cyclic voltammetry (CV) test was operated at a scanning rate of 0.1 mV·s^{-1} between 3.6 V and 5.0 V (vs Li/Li^+).

2 Results and discussion

Fig.2 shows the TG-DTG-DTA curves of Sample A precursor from 30 ℃ to 975 ℃.From the illustration, it can be seen that the primary weight-loss interval exists between 30 ℃ and 420 ℃. When the temperature exceeds 420 ℃, just small mass loss can be seen, which demonstrates that all of the organic components decomposed completely. The mass loss region between 30 ℃ and 420 ℃ can be divided in three mainly steps. The first step lies in 30 ℃ to 190 ℃(with a peak of weight loss at 168.9 ℃), which can be ascribed to the evaporation of free and crystal water. The second step is located between 190 ℃ and 305 ℃, corresponding to the decomposition of nitrate as well as the carbonizing process of sucrose and acetate (with a peak of mass loss at 250.8 ℃). The greatest degree of weight loss occurred in the third region (*ca.* 305~420 ℃), which can be attributed to the completely combustion of carbon and the residual nitrate and acetate. From the c-DTA curve, this process is also accompanied with a massive heat releasing, which indicates the preliminary crystallization of $LiCr_{0.2}Ni_{0.4}Mn_{1.4}O_4$ products. After that, the spinel structure particles composed of Li, Ni, Mn, Cr ions start to grow, thus almost no weight loss could be observed after 420 ℃. As heating temperature continue to increases, an indistinguishable decrease occurs on the TG curve (mass loss of 1.27%). This phenomenon might be due largely to the oxygen deficiency during the high-temperature sintering process ($LiCr_{0.2}Ni_{0.4}Mn_{1.4}O_{4-\delta}$). Therefore, the cubic spinel structure of as-synthesized materials possibly dominated by $Fd\bar{3}m$ space group (face-centered), and their do exist a small amount of Mn^{3+} in the spinel structure that is caused by the charge balance, which can be proved by the analyses of

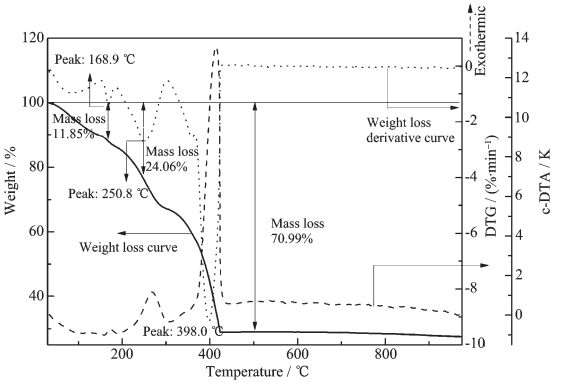

Fig.2 TG-DTG-DTA curves of Sample A precursor

following figures.

The results of X-ray patterns of the prepared samples are shown in Fig.3. The diffractograms of both samples can be well matched with the spinel structure of $LiNi_{0.5}Mn_{1.5}O_4$ found in the JCPDS#80-2162, which signifies that Ni and Mn were completely replaced by Cr. The calculated crystallinities of both samples are 98.70% and 96.53%, respectively. However, a minor trace of $Li_xNi_{1-x}O$[25-26] could be observed at the peak of 44° of Sample B, which may be ascribed to its slight heterogeneous phase distribution existing in the thermo polymerization process which can lead to the generation of impurities. The lattice parameters of Sample A and B calculated by Jade6.5 software are 0.816 0 nm and 0.816 2 nm, respectively, both of which are less than theoretical value (0.817 3 nm)[27]. What may causes the results is that certain amount of Ni^{2+} (0.065 nm) was replaced by Cr^{3+} (0.062 nm) of both samples. In Sample B, little more quantity of Mn^{3+} (0.064 5 nm) generated than that of Sample A, therefore the value of lattice parameter of Sample B is larger (ionic radius of Mn^{4+} is 0.053 0 nm). This occurence may be due to the principle of electroneutrality that leads to the different levels of charge compensations caused by the different degrees of oxygen losses. Appropriate quantity of Mn^{3+} within the spinel structure ($LiCr_{0.2}Ni_{0.4}Mn_{1.4}O_{4-\delta}$) can provide a convenient passway for lithium ion transference and promote electrochemical performances significantly[28-30].

From the SEM images shown in Fig.4a~d, we can see that both samples appear cubic spinel morphology and are composed of good dispersivity nano-or submicron-crystals. The particles size distributions of the two samples detected by JL-6000 Dry Powder Laser Particle Sizer are presented in Fig.4e, f, and the average particle size (D50) of Sample A and B are estimated to be 0.562 μm and 0.649 μm, respectively. Appropriate particle size of high voltage material has a nonnegligible influence both on cyclic performance and rate capability[9]. The particles of both samples are well crystallized spinel structures, but it is obvious that some crystals are imperfect in Sample B (Fig.4d). The reason for the imperfection can be ascribed to the generation of impurities, and the sample without high-vacuum device could not disperse at an ideal condition during the thermal polymerization process, which makes the spinel particles within impurities easily melted at a high temperature.

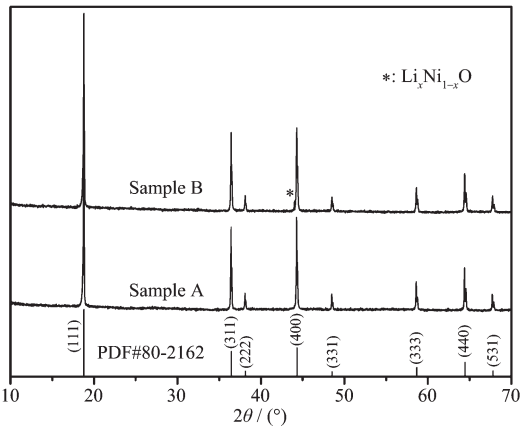

Fig.3　X-ray diffraction patterns of Sample A and Sample B

The specific capacities of as-prepared samples at different discharge rates (from 1C to 20C) were investigated in detail (1C=147 mAh·g^{-1}). From Fig.5c it can be seen that the maximum obtainable discharge capacities of Sample A at 1C, 3C, 5C, 10C, 20C are 140.5, 126.9, 124.7, 121.0, and 117.3 mAh·g^{-1}, respectively. As shown In Fig.5a, both samples exhibit excellent rate capabilities, and Sample B can also deliver a discharge capacity of 105 mAh·g^{-1} under 20C, which has capacity retention of 77.8% relative to its initial discharge capacity. (This value of Sample A is 83.2%). Fig.5b exhibits the 3th and 30th charge-discharge curves of Sample A at a discharge rate of 1C, and no obvious variation of the primary discharge plateau could be observed. To further detect the cyclic properties, the cells of both samples were cycled for 100 times at discharge rates of 1C and 10C. The test results illustrate that the $LiCr_{0.2}Ni_{0.4}Mn_{1.4}O_4$ cathode materials show excellent cyclic stability (Fig.5d). The capacity retentions of Sample A and Sample B at 1C (10C) can reach up to 96.6%, 95.4% (96.9%, 96.4%), respectively. From Fig. 5e it can be seen that Sample A exhibits higher energy density than that of Sample B at different current densities. What's more, it's worth noting that

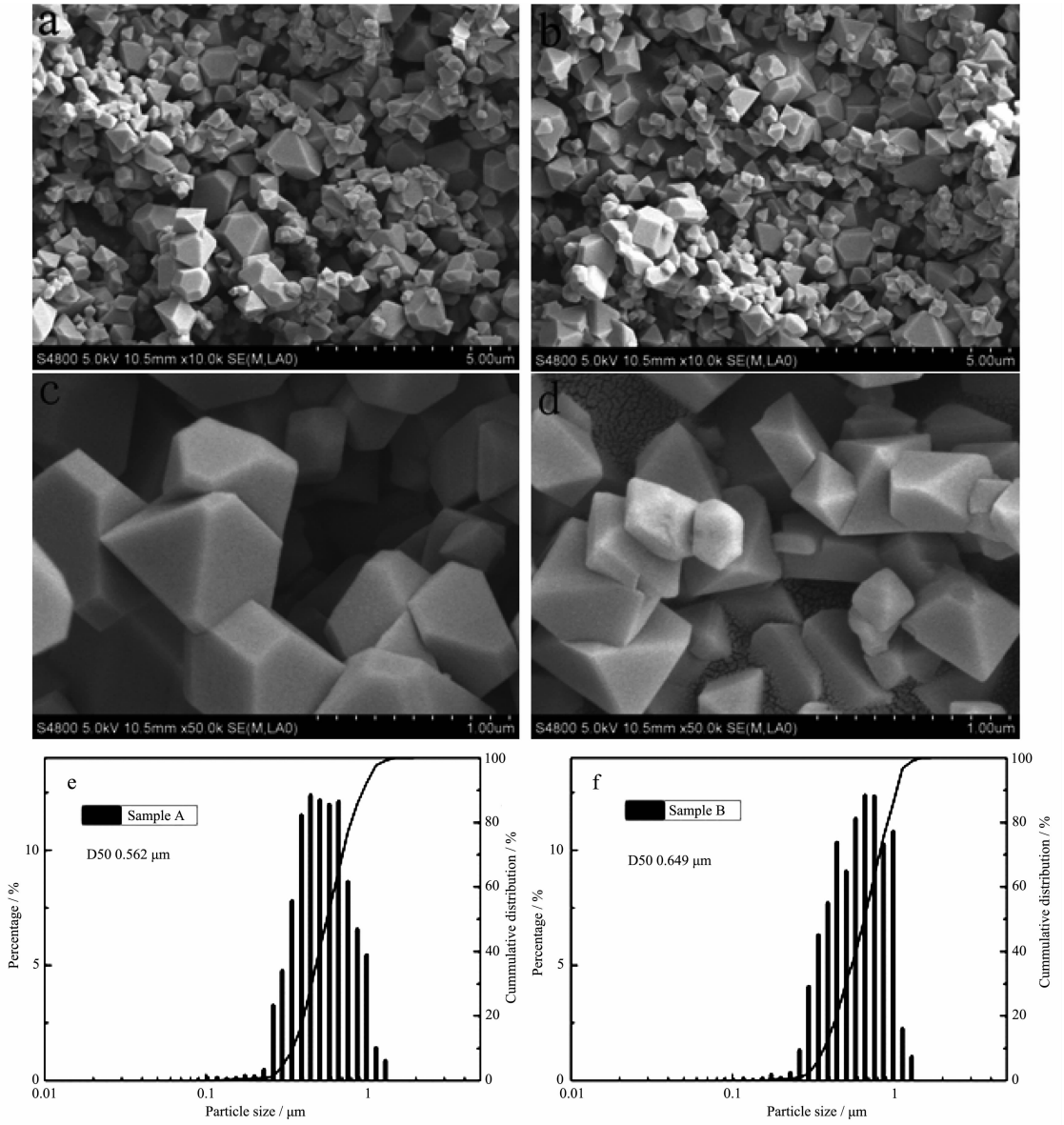

Fig.4 SEM images of (a), (c) Sample A and (b), (d) Sample B; (e), (f) Corresponding particle size histograms of the two samples

the as-prepared material could deliver an energy density of 640.4 $Wh \cdot kg^{-1}$, which can be calculated by the integral area of discharge capacity curve. It is also very close to the theoretical value (686 $Wh \cdot kg^{-1}$)[31], and its overall average working voltage is 4.56 V , which can be figured out via dividing energy density by discharge capacity. Such a high energy density enables it to be a very promising cathode material for the next generation of high power lithium ion batteries.

One important factor that affects the cyclic stability performance is the bonding energies on neighbouring atoms. Just as already stated previously, the bonding energy of Cr-O (461 $kJ \cdot mol^{-1}$) is stronger than that of Ni-O (382 $kJ \cdot mol^{-1}$) and Mn-O (402 $kJ \cdot mol^{-1}$), which can provide a sturdy framework of spinel particles. Besides, the appropriate voltage window (3.6 ~5.0 V) also plays a significant role for the cyclic property. In addition, the high crystallinities of as-synthesized samples (as shown in XRD patterns) also contribute to the cyclic performances.

Fig.6 shows the discharge curves of both samples with increasing discharge rates. As is shown in Fig.6a and Fig.6b, two primary discharge plateaus (around 4.6 V and 4.7 V) and a tiny discharge plateau of 4.0 V emerge at 1C, corresponding to the redox couples of

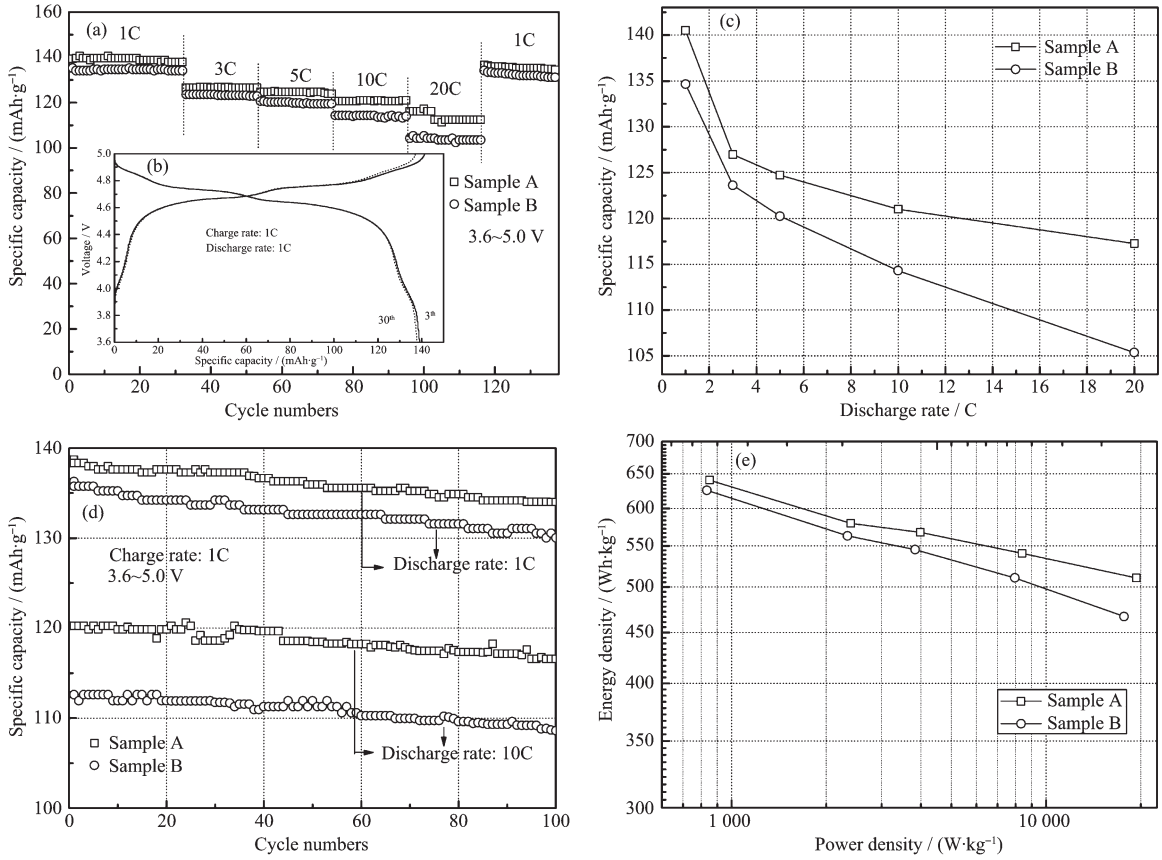

Fig.5　(a) Rate performances of Sample A and Sample B at different discharge rates; (b) (Inset) Charge-discharge curves of 3th and 30th at 1C; (c) Rate properties for both samples at C-rate varying from 1C to 20C; (d) Cyclic stability performances of Sample A and Sample B at 1C and their high rate cyclic stability performances at 10C; (e) Ragone plot for both samples

Ni^{2+}/Ni^{3+}, Ni^{3+}/Ni^{4+} and Mn^{3+}/Mn^{4+}, which demonstrates that the charge-discharge processes are involved in the multi-phase reactions. Furthermore, to a certain degree, the oxygen loss of the previous analysis of TG curve could be confirmed by the appearance of Mn^{3+}/Mn^{4+} plateau. The intervals of Sample A are smaller than those of Sample B, indicating the higher discharge capacities of Sample A under all discharge current densities.

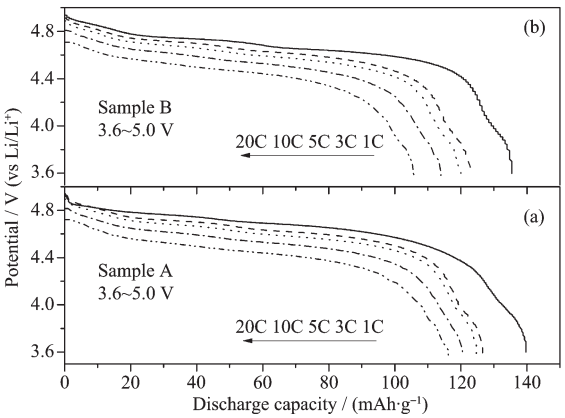

Fig.6　Discharge curves at different rates of (a) Sample A and (b) Sample B

Fig.7 shows the cyclic voltammetry (CV) curves of Sample A and Sample B in the potential range from 3.6 V to 5.0 V with a scanning rate of 0.1 $mV \cdot s^{-1}$. As shown in Fig.7a, three primary peaks emerge around 4.1 V, 4.7 V, 4.8 V, corresponding to the redox couples of Mn^{3+}/Mn^{4+}, Ni^{2+}/Ni^{3+}, Ni^{3+}/Ni^{4+}, respectively. For Sample A, the redox peaks of the electrode are stronger than those of Sample B, indicating the better electrochemical property and lower resistance of Sample A. Apart from the three dominating reversible peaks mentioned above, one redox peak around 4.9 V occurs, corresponding to the Cr^{3+}/Cr^{4+} couple. Moreover, more amount of Mn^{3+}do exist in Sample B than that in Sample A, which is illustrated in Fig.7b. This phenomenon could just confirm the inference that

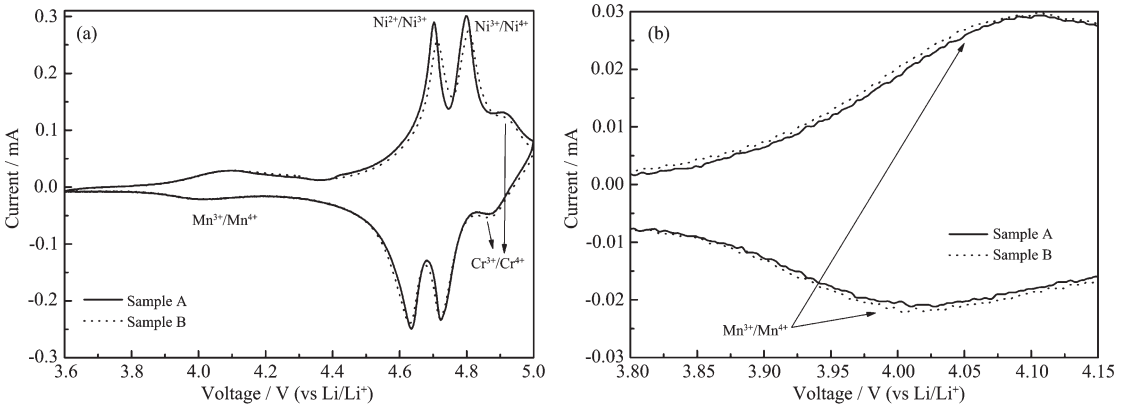

Fig.7 (a) Cyclic voltammetry (CV) curves of Sample A and Sample B, (b) CV curves in the voltage range of 3.8~4.15 V for both samples

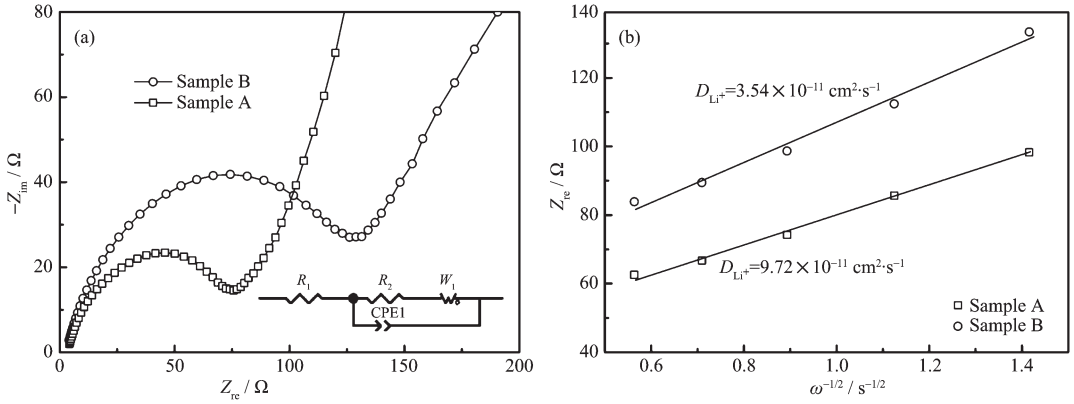

Fig.8 (a) A.C. impedance spectra of Sample A and Sample B; (b) Relationship between impedance and low frequency region, and the diffusion coefficients of Li^+ for both samples

there are a little more amount of Mn^{3+} in Sample B (as is analyzed by TG curve and XRD patterns) which is caused by the principle of electroneutrality (as a consequence of different levels of oxygen deficiency).

EIS is used for analysising the electrochemical characteristics affected by the different methods, and it is also a potent technique to calculate the diffusion coefficient of Li^+. Fig.8a is the Nyquist plots of Sample A and Sample B, and the equivalent circuit for simulating the spectra is shown inset. The spectra of both samples consist of three main sections, (a) the electrolyte resistance (R_1); (b) the surface and charge transfer resistance (R_2); (c) the Warburg resistance (W_1) which is associated with the diffusion coefficient of Li^+. The CPE_1 in parallel with R_2 and W_1 represents the electric double layer capacitance. The resistance values of different sections calculated by ZView2 software are exhibited in Table 1.

For the two samples, the values of R_1 only changed a little; however, large variations on the values of R_2 took place. The alteration of Sample B demonstrate that the SEI (solid-electrolyte interface) formed on the cathode surface may become thicker by consuming active Li ion[32]. This phenomenon may ascribe to (a) the worse compatibility of electrolyte and cathode material interface caused by the impurities, and (b) more formed Mn^{3+} could decrease the structural stability of the face-centered cubic spinel particles[33]. Together, to some extent, the pathways for Li^+ (Li ions are supposed to transfer to 8a tetrahedral sites and 32e site) are partially hindered or lengthened, thus the R_2 of Sample B increased

Table 1 Calculated values of different resistances and diffusion coefficients of Li^+

Sample	R_1 / Ω	R_2 / Ω	D_{Li} / ($cm^2 \cdot s^{-1}$)
A	2.021	59.46	9.72×10^{-11}
B	2.123	95.22	3.54×10^{-11}

compared with Sample A.

The diffusion coefficients of lithium ions can be figured out based on the following equation[7,34]:

$$D_{Li}=\frac{R^2T^2}{2A^2n^4F^4c^2\sigma^2}$$

In this formula, R is the gas constant ($J\cdot mol^{-1}\cdot K^{-1}$), T is Kelvin temperature in K, A stands for the loading area of cathode materials (cm^2), n is the charge transfer number (n=1), F represents the Faraday constant in $C\cdot mol^{-1}$, and c is the concentration of Li^+ ($mol\cdot cm^{-3}$). The results are shown in Table 1, indicating that Sample A has a larger diffusion coefficient of Li^+ compared with Sample B. The higher diffusion coefficient of Li^+ and lower surface charge transfer resistance (R_2) could alleviate the polarization, increase the electrical conductivity, and promote the electrochemical performance effectively.

3 Conclusions

In this work, Cr-doped spinel $LiCr_{0.2}Ni_{0.4}Mn_{1.4}O_4$ were first prepared by a low-temperature solvothermal method. Among conventional solvothermal routes, excess solvent just evaporates near its boiling point without involving the influences of saturated vapor pressure and generated bubbles on invisible particles. Larger numbers of bubbles are generated by lower saturated vapor pressure, which provides a more completely thermal polymerization process and avoids the possible deposition phenomenon. Via the low-temperature solvothermal method, high degree of crystallinity of spinel particles could be obtained. From TG and CV curves it can be inferred that a small amount of Mn^{3+} ions formed during the high temperature calcination process, and the space group of obtained particle is dominated by $Fd\bar{3}m$ (face-centered) with well-shaped morphology and a comparative uniform size distribution. In the potential window of 3.6~5.0 V, desirable discharge capacity of 140.5 $mAh\cdot g^{-1}$ at 1C could be obtained, as well as an energy density of 640.4 $Wh\cdot kg^{-1}$. It also reveals the excellent cycle stability of the prepared samples with high capacity retentions of 96.6% and 96.9% separately at 1C and 10C after 100 cycles. The EIS results show that samples synthesized by low-temperature solvothermal method have lower surface and charge resistance, and higher diffusion coefficients of lithium ions. This study demonstrates that the as-synthesized Cr-doped $LiCr_{0.2}Ni_{0.4}Mn_{1.4}O_4$ cathode material exhibits enhanced electrochemical performances and high energy density, which provides a low energy consuming approach for the industrialization of this high power and high energy cathode material.

Acknowledgements: This work is supported by the Youth Foundation of Sichuan University (No.2011SCU11081), the research fund for the Doctoral Program of Higher Education, the Ministry of Education (No.20120181120103), and Open Engineering Project for Phosphorus chemical Industry of National Engineering Centre (No.2013LF1012). The Biological material analysis and test center of Sichuan University also provided supports for us.

References:

[1] Park J S, Roh K C, Lee J W, et al. *J. Power Sources*, **2013**, **230**:138-142

[2] Li B, Xing L, Xu M, et al. *Electrochem. Commu.*, **2013**,**34**: 48-51

[3] Sha O, Wang S, Qiao Z, et al. *Mater. Lett.*, **2012**,**89**:251-253

[4] Kim J H, Pieczonka N P W, Li Z, et al. *Electrochim. Acta*, **2013**,**90**:556-562

[5] Liu G Q, Wen L, Liu G Y, et al. *J. Alloys Compd.*, **2010**, **501**:233-235

[6] Aklalouch M, Amarilla J M, Rojas R M, et al. *J. Power Sources*, **2008**,**185**:501-511

[7] Nie X, Zhong B, Chen M, et al. *Electrochim. Acta*, **2013**,**97**: 184-191

[8] Yi T F, Shu J, Zhu Y R, et al. *J. Phys. Chem. Solids*, **2009**, **70**:153-158

[9] Aklalouch M, Rojas R M, Rojo J M, et al. *Electrochim. Acta*, **2009**,**54**:7542-7550

[10]Zhang X, Cheng F, Zhang K, et al. *RSC Adv.*, **2012**,**2**:5669-5675

[11]Fang X, Ding N, Feng X Y, et al. *Electrochim. Acta*, **2009**, **54**:7471-7475

[12]Yang T, Sun K, Lei Z, et al. *J. Solid State Electrochem.*, **2010**,**15**:391-397

[13]Hwang B J, Wu Y W, Venkateswarlu M, et al. *J. Power*

Sources, **2009**,**193**:828-833

[14]HE Ze-Qiang (何则强), XIONG Li-Zhi(熊利芝), WU Xian-Ming(吴显明), et al. *Chinese J. Inorg. Chem.*(无机化学学报), **2007**,**23**(5):875-878

[15]Feng X Y, Shen C, Fang X, et al. *J. Alloys Compd.*, **2011**, **509**:3623-3626

[16]JI Yong(季勇), WANG Zhi-Xing(王志兴), YIN Zhou-Lan (尹周澜), et al. *Chinese J. Inorg. Chem.*(无机化学学报), **2007**,**23**(4):597-601

[17]NIE Xiang (聂翔), GUO Xiao-Dong (郭孝东), ZHONG Ben-He(钟本和), et al. *Chinese J. Inorg. Chem.*(无机化学学报), **2012**,**28**(12):2573-2580

[18]FAN Wei-Feng(范未峰), QU Mei-Zhen(瞿美臻), PENG Gong-Chang(彭工厂), et al. *Chinese J. Inorg. Chem.*(无机化学学报), **2009**,**25**(1):124-128

[19]Kim J H, Myung S T, Sun Y K, et al. *Electrochim. Acta*, **2004**,**49**:219-227

[20]Choi S H, Hong Y J, Kang Y C, et al. *Nanoscale*, **2013**,**5**: 7867-7871

[21]Etacheri V, Marom R, Elazari R Salitra G, et al. *Energy Environ. Sci.*, **2011**,**4**:3243-3262

[22]Kraytsberg A, Ein-Eli Y. *Adv. Energy Mater.*, **2012**,**2**:922-939

[23]Braun P V, Cho J, Pikul J H, et al. *Curr. Opin. Solid State Mater. Sci.*, **2012**,**16**:186-198

[24]Fergus J W. *J. Power Sources*, **2010**,**195**:939-954

[25]Jin Y C, Duh J G. *Mater. Lett.*, **2013**,**93**:77-80

[26]Liu G Q, Wen L, Wang X, et al. *J. Alloys Compd.*, **2011**, **509**:9377-9381

[27]Sha O, Qiao Z, Wang S, et al. *Mater. Res. Bull.*, **2013**,**48**: 1606-1611

[28]Ariyoshi K, Iwakoshi Y, Nakayama N, et al. *J. Electrochem. Soc.*, **2004**,**151**:A296-A303

[29]Jin Y C, Lin C Y, Duh J G. *Electrochim. Acta*, **2012**,**69**:45-50

[30]Xiao J, Chen X, Sushko P V, et al. *Adv. Mater.*, **2012**,**24**: 2109-2116

[31]Zhong G B, Wang Y Y, Zhang Z C, et al. *Electrochim. Acta*, **2011**,**56**:6554-6561

[32]Pieczonka N P W, Liu Z, Lu P, et al. *J. Phys. Chem. C*, **2013**,**117**:15947-15957

[33]Shu J, Yi T F, Shui M, et al. *Comput. Mater. Sci.*, **2010**,**50**: 776-779

[34]Seyyedhosseinzadeh H, Mahboubi F, Azadmehr A. *Electrochim. Acta*, **2013**,**108**:867-875